Zeitschrift für Physikalische Chemie, **215**, 6, 717–735 (2001)

Picosecond IR Study of UV-Induced Peroxide Decomposition: Formation and Vibrational Relaxation of CO_2 in CH_2Cl_2 Solution

By Michael Buback*, Matthias Kling, Marco Thomas Seidel, Frank Dieter Schott, Jörg Schroeder * and Ulrich Steegmüller

Institut für Physikalische Chemie der Universität Göttingen, Tammannstr. 6, D-37077 Göttingen, Germany

Dedicated to Prof. Dr. Dr. h.c. mult. J. Troe on the occasion of his 60th birthday

(Received August 3, 2000; accepted September 20, 2000)

Picosecond UV pump (248.5 nm)/IR probe spectroscopy has been applied to the study of the decomposition of several aromatic diacyl peroxides, peroxycarbonates, and of a peroxyester dissolved in CH_2Cl_2. Measuring the IR transient absorbance in the 2100 to 2450 cm^{-1} range allows to monitor the formation and vibrational relaxation of the photoproduct CO_2 via the asymmetric stretching mode (ν_3) with a time resolution of 1.8 ps. With each of the six peroxides a CO_2 molecule is released at delay times below 10 ps. The energy relaxation of the initially formed vibrationally hot CO_2 is followed over the time range up to 500 ps. Analysis of the transient IR spectra, via an anharmonic oscillator model proposed by Hamm *et al.* [1], shows a monoexponential decay of internal energy. Irrespective of the type of peroxide a single relaxation time of 67 ± 5 ps is found to adequately represent the cooling behavior of CO_2 in liquid CH_2Cl_2. The "initial" temperatures of vibrationally hot CO_2 at a delay time of 20 ps after applying the pump pulse differ considerably, between 1400 and 2700 K for the decompositions of *tert*-butyl benzoyl peroxide and *tert*-butyl benzoyl carbonate, respectively. These remarkably high temperatures are assumed to originate from energy release associated with structural relaxation of the bent OCO moiety to form the linear CO_2 molecule.

Introduction

Peroxides are widely used as initiators in free-radical polymerizations [2]. Reliable rate coefficients for thermally and photochemically induced peroxide decomposition are required for modeling polymerization processes. A large body of literature on the decomposition kinetics of organic peroxides has accumulated [3]. Nevertheless, the mechanistic details of their decomposition dy-

* Corresponding authors. E-mail: mbuback@gwdg.de, jschroe2@gwdg.de

namics are not yet adequately understood. Particular interest centers around the mode of bond scission in peroxides which upon decomposition release a stable small molecule, such as carbon dioxide. The primary dissociation event in peroxyesters, diacyl peroxides, and peroxycarbonates may be either the scission of the O−O bond (with subsequent decarboxylation of the OCO containing intermediate) or concerted two-bond scission associated with the instantaneous release of CO_2. Picosecond UV pump/IR probe experiments are perfectly suited for the analysis of such processes, as the formation of CO_2 can be monitored directly via the transient absorbance of the asymmetric stretching mode (ν_3).

Among the four peroxides studied so far by this technique with excitation at 308 nm, *tert*-butyl-peroxy-2-naphthylcarbonate (TBNC) was found to decompose in a stepwise manner with a CO_2 formation time of 31 ps [4], whereas for di(1-naphthoyl) peroxide [4], di(2-naphthoyl) peroxide [5], and for *tert*-butyl-9-methylfluorene-9-percarboxylate [6] CO_2 appeared within the experimental time resolution of 1.8 ps, suggesting concerted bond scission.

As the absorptivity of most peroxides is fairly low at 308 nm, it appeared mandatory to modify the experimental system such that UV excitation may be carried out at shorter wavelengths. The present paper illustrates the modification of the assembly for UV excitation at 248.5 nm, which allowed us to carry out pump/probe experiments on dibenzoyl peroxide (DBPO), di(4-methoxy benzoyl) peroxide (DMBP), *tert*-butyl benzoyl peroxide (TBPB), and *tert*-butyl benzoyl carbonate (TBBC). In order to study the effect of excitation energy, *tert*-butyl-peroxy-2-naphthylcarbonate (TBNC) [4] and di(2-naphthoyl) peroxide (DNPO) [5] which have already been investigated at an excitation wavelength of 308 nm, were reinvestigated at 248.5 nm. The structures of the individual peroxides are given in Scheme 1. As can be seen in this scheme, DBPO, DMBP and DNPO belong to the diacyl peroxide family whereas both TBBC and TBNC are peroxycarbonates. It should be noted that the diacyl peroxides contain two –C(O)O– moieties which may release CO_2. Within the present study only the formation of the first CO_2, which occurs in the ps or sub-ps range, is of interest. With diacyl peroxides a second CO_2 molecule may be released by thermal decarboxylation of the intermediate aroyloxy free radical. This process occurs on the ns to μs time scale and has already been investigated by UV pump/VIS probe and EPR experiments [7].

The modes of bond scission are illustrated in Scheme 2. k_1 refers to the rate coefficient for single-bond scission, whereas k_{con} denotes the rate coefficient for concerted two-bond scission. k_{rec} and k_2 characterize the recombination and decarboxylation rates of the intermediate free radical, respectively. Beyond the fundamental interest to understand the detailed mechanism of the unimolecular fragmentation process, the mode of dissociation, sequential or concerted, may strongly influence initiator efficiency in the technical process of free-radical polymerization. In addition to studying the mode of bond scission, the dynamics of energy relaxation for the reaction

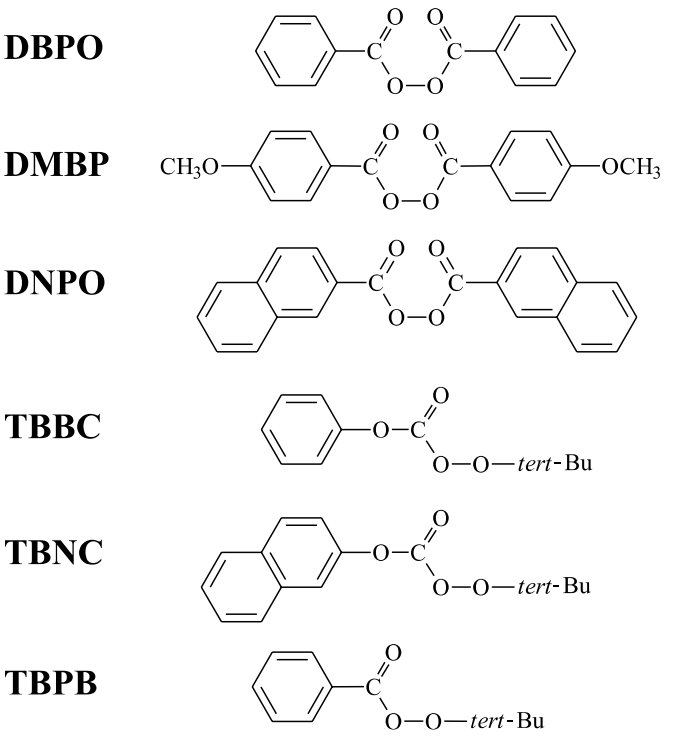

Scheme 1. Peroxides under investigation: dibenzoyl peroxide (DBPO), di(4-methoxy benzoyl) peroxide (DMBP), di(2-naphthoyl) peroxide (DNPO), *tert*-butyl benzoyl carbonate (TBBC), *tert*-butyl-peroxy-2-naphthoylcarbonate (TBNC) and *tert*-butyl benzoyl peroxide (TBPB).

products is also fundamental to the understanding of unimolecular reactions. By monitoring the time evolution of the IR-band shape of the asymmetric stretching mode (ν_3), such relaxation measurements may be carried out on CO_2. The preceding UV pump/IR probe studies provided clear evidence for the production of vibrationally hot CO_2 (*vide infra*). The CO_2 spectra measured in CCl_4 are in close agreement with data determined on vibrationally hot CO_2 in shock waves [8], in heated gas cells [9], and in supersonic burners [10]. To deduce a vibrational temperature from the transient spectra, an anharmonic oscillator model applied by Hamm *et al.* appears to be perfectly suited [1]. Vibrational relaxation in condensed fluid phase has been extensively studied during recent years [11–13], but information about the energy relaxation of highly excited small polyatomic molecules like CO_2 in solution is scarce [12, 14]. To the best of our knowledge we report for the first time on energy tranfer of vibrationally excited CO_2 in a polar liquid.

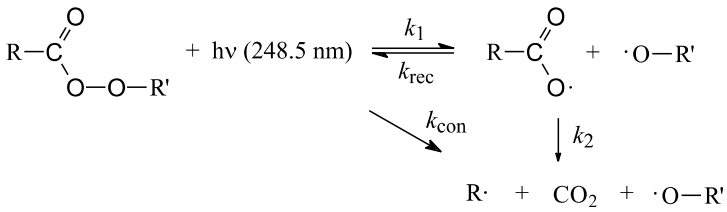

Scheme 2. Reaction scheme for the photoinduced peroxide decarboxylation: diacyl peroxide (R = aryl, R′ = aroyl); peroxyester (R = aryl, R′ = *tert*-butyl), and peroxycarbonates (R = aryloxy, R′ = *tert*-butyl); for explanation of the rate coefficients, *k*, see text.

Experimental section

The experimental setup for the time-resolved study of peroxide decomposition induced by UV pump pulses at 308 nm and monitored via tunable IR probe pulses in the 2000 to 5000 cm^{-1} region was described previously [15]. This device was modified for excitation at 248.5 nm. The main components and characteristics of the new UV pump/IR probe spectrometer are illustrated in Fig. 1.

The oscillator tube (filled with 70 mbar Xe, 90 mbar HCl (5% in He) and 2.34 bar Ne) of a twin tube excimer laser (Lambda Physik EMG 150E) is op-

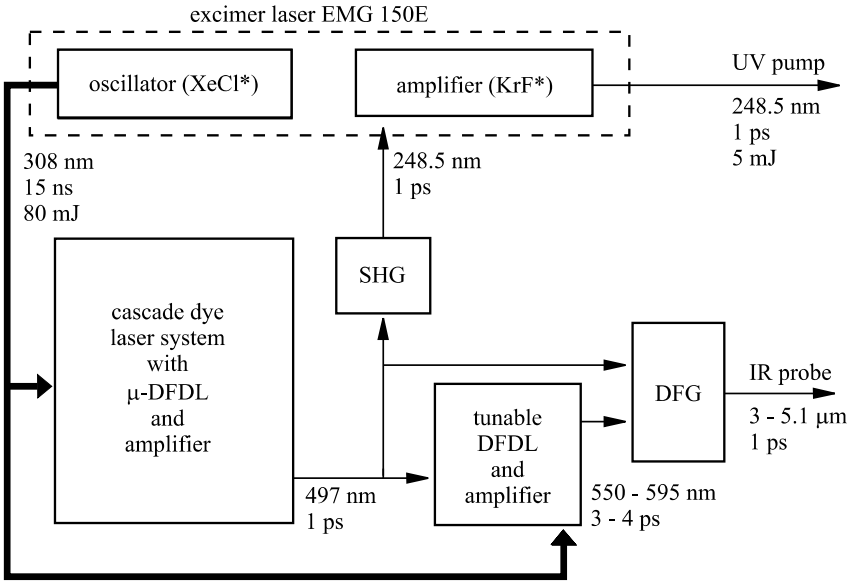

Fig. 1. Schematic view of the laser setup with SHG: second harmonic generation, DFDL: distributed feedback dye laser and DFG: difference frequency generation.

erated on the XeCl* line at 308 nm with a repetition rate of 10 Hz. The laser radiation pumps a cascade dye laser system containing a distributed feedback dye laser (μ-DFDL) [16]. The μ-DFDL (0.1 M solution in dimethyl formamide of the dye C307) provides laser pulses of about 1 ps width at 497 nm. These pulses were amplified to 150 μJ by passing twice through both an off-axis amplification cell [17] (7 mM solution in propylene carbonate of the dye C102) and a Bethune type [18] cell (3 mM solution in ethanol of the dye C307) with a 2 mm bore.

The fundamental pulses at 497 nm were used for second harmonic generation (SHG) in a 0.3 mm thick BBO crystal (cut at an angle of 53° relative to the optical axis). Double pass amplification in the second tube of the excimer laser operated on the KrF* line (gas mixture: 150 mbar Kr, 120 mbar F_2 (5% in He) and 1.83 bar He) provides UV pump pulses at 248.5 nm with single pulse energies up to 5 mJ. Pulse-to-pulse fluctuations are less than 5% and the amplified spontaneous emission background is below 10%.

The remainder of the fundamental pulse at 497 nm (from SHG) serves for pumping the prismatic DFDL [19] and for difference frequency generation (DFG). The tunable prismatic DFDL, which was originally developed for the emission range between 700 and 850 nm by Jasny [15], has been modified, again in cooperation with Jasny, for the tuning range from 550 to 595 nm. This modification required the construction of a laser cuvette with a front prism made from fused silica at an angle of 60°. Also the diffraction grating had to be changed, to 1400 lines/mm (blazed at 500 nm). The tunable wavelength range from 552 to 566 nm is obtained with only one dye solution (5.8 mM solution in 1,1,1,3,3,3-hexafluoro-2-propanol of the dye R6G). This signal pulse is amplified in an off-axis cell (13 mM solution in propylene carbonate of the dye C153) to an energy of around 0.5 μJ at pulse durations of 3 to 4 ps.

IR probe wavelengths ranging from 3 to 5.1 μm are produced by DFG with type-I phase matching of signal and fundamental pulses in a $LiIO_3$ crystal of 5 mm thickness (cut at an angle of 22° with respect to the optical axis). Phase matching upon changing signal wavelength was achieved by a computer controlled rotation unit. Visible pulses behind the DFG are blocked with Si plates (Fig. 2) adjusted at the Brewster angle (73.7°). The IR probe pulses are focused (lens L2, $f = 300$ mm) on a Ge beamsplitter, which divides the IR beam into a sample and a reference beam of equal energy. Sample (S) and reference (R) beam are transmitted through identical stainless steel flow cells with 100 μm optical path length.

The UV pump and IR probe beams overlap under an angle of 10° with the focus of the UV beam (lens L1, $f = 1000$ mm) being slightly behind the sample cell. The polarization between pump und probe pulses was adjusted to 54.7° (magic angle) with a $\lambda/2$ plate. Delay times between pump and probe pulses were adjusted by a computer controlled translation stage. By means of a dielectric mirror (DM) pump energy was reduced to 2 mJ in order to avoid transient

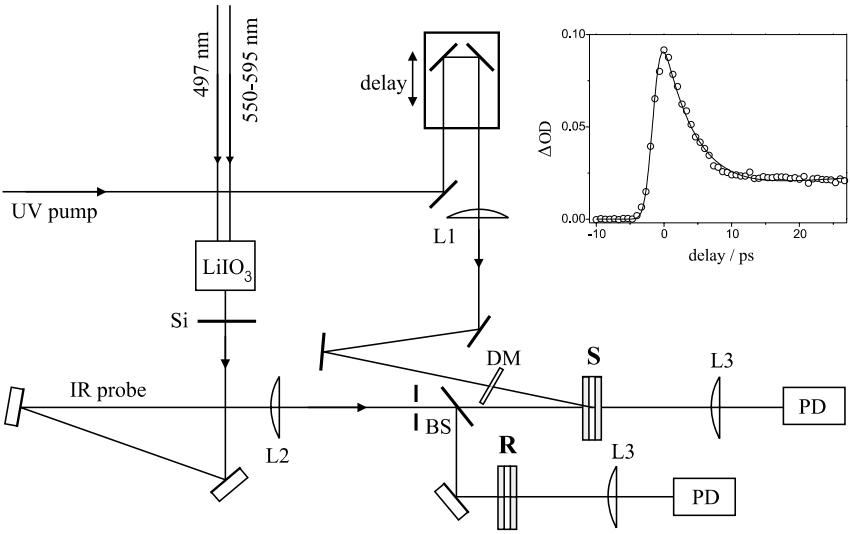

Fig. 2. Schematic view of the pump/probe assembly with DM: dielectric mirror, BS: beamsplitter, PD: photodetector, S: sample cell and R: reference cell.; Inset: transient IR absorption of Germanium at 2300 cm^{-1} after excitation at 248.5 nm (see text).

signals and damage at the front window (MgF_2, 2 mm thick) of the sample cell. The backside window of the sample cell and both windows of the reference cell consisted of 5 mm thick CaF_2.

Probe and reference IR beams were collimated with CaF_2 lenses (L3, $f = 100$ mm) and focused onto liquid-nitrogen-cooled InSb photo-detectors PD (EG&G J10D M-204). Electronic signals from the photodiodes were amplified and digitized with an A/D converter. Typically 50 individual laser shots were averaged to obtain a single absorbance data point for either constant delay time or constant wavenumber. The detection limit for changes in optical density was about $\Delta OD = \pm 0.001$.

The cross-correlation width and the zero point delay between pump and probe pulses were deduced by independently measuring the transient absorption of Ge plates at 2300 cm^{-1} after excitation at 248.5 nm. Experimental data points together with a simulated curve are shown in the inset in Fig. 2. The simulation consists of a convolution of the system response with the Gaussian cross-correlation function. From the rise time of the absorption measurement, a time resolution for the pump/probe experiment of 1.8 ps has been deduced. The spectral width of the IR pulses is 10 to 12 cm^{-1}, the wavenumber accuracy is ± 5 cm^{-1}. The precision within one experimental spectrum is better than ± 1 cm^{-1}.

The peroxide samples (Scheme 1) were synthesized and provided by AKZO Nobel (Research Center Deventer, The Netherlands) in high purity.

With CH_2Cl_2 (Merck, Uvasol) being used as the solvent, the transient signals at high pump intensities were very small. The entire set of experiments was carried out at ambient pressure and temperature. The concentration of the sample solutions was adjusted to an optical density at the pump wavelength of OD(248.5 nm) = 10 for di(2-naphthoyl) peroxide (DNPO) and of OD (248.5 nm) = 2 for the other peroxides. Under these conditions, the number of molecules in the pumped volume exceeds the number of photons in the pump pulse by at least a factor of 10, which assures that bleaching effects will not occur.

Results

Transient IR absorption measured after ps photo-excitation of *tert*-butyl benzoyl carbonate (TBBC) in CH_2Cl_2 at delay times between −40 and 500 ps are shown in Fig. 3. Decay curves were measured at fixed wavenumber every 20 cm^{-1} across the ν_3-band and combined to yield the 3-dimensional plot shown in Fig. 3. Transient background absorption by the solvent and the window material were subtracted according to the procedure described below.

At negative delay times the signal is dominated by fluctuations within the detection limit of $\Delta OD = \pm 0.001$. Slightly enhanced transient signals occur between 2320 and 2350 cm^{-1}. They are due to effects of atmospheric CO_2 on the pulse profile [20]. At zero delay time, an instantaneous rise in optical density is seen in the spectral range from 2170 to 2330 cm^{-1}. With increasing delay time the absorption band simultaneously shifts to higher wavenumbers and narrows. After 500 ps the band maximum is located at 2335 cm^{-1} (with a spectral width of 19 cm^{-1}) with this position being in good agreement with the one measured for a stationary CO_2 spectrum in CH_2Cl_2 at ambient temperature. Studying the same solution in an FTIR spectrometer (Bruker IFS 88) yields a band maximum position of 2338 cm^{-1} and a band width of 8 cm^{-1}, which is in full agreement with literature values [21]. The difference in the absolute band position is within the limits of accuracy of the ps spectrometer. The spectral width of the ps band is reproduced by convolution of the FTIR band profile with the spectral broadening function of the ps IR pulses (11 cm^{-1}). The measured absorption band at longer delay times thus can unambiguously be assigned to the dissociation product CO_2.

Fig. 4 shows spectra measured at delay times of 20, 100, and 500 ps after photolysis of TBBC in CH_2Cl_2. The lines fitted to the data will be explained in the discussion section. Shifting and broadening of CO_2 absorption as in Figs. 3 and 4 was observed for all peroxides under investigation. Absorption bands recorded at delay times greater than 300 ps remain unchanged for all peroxides.

At wavenumbers between 2410 and 2450 cm^{-1}, time dependent signals were observed which could not be assigned to the absorption of CO_2. Fig. 5 shows signals for this range as a function of delay time after photolysis of

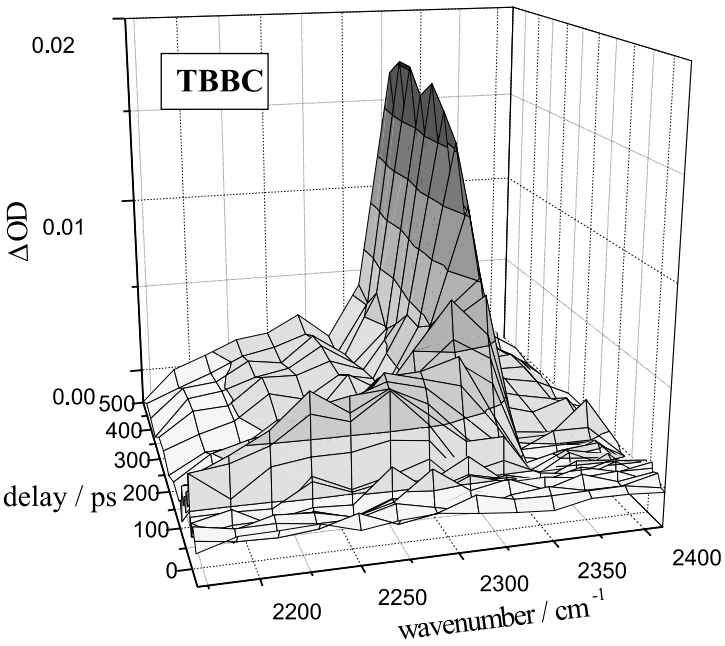

Fig. 3. Temporal (−40 to 500 ps) and spectral (2170 to 2410 cm^{-1}) evolution of the ν_3 absorbance (optical density) of CO_2 after UV-induced decomposition of TBBC in CH_2Cl_2.

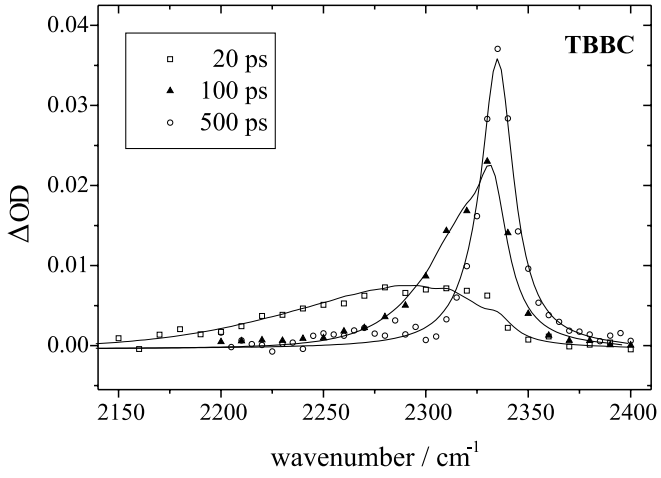

Fig. 4. Transient spectra of the ν_3 absorbance of CO_2 at three delay times (20, 100, and 500 ps) after UV-induced decomposition of TBBC in CH_2Cl_2.

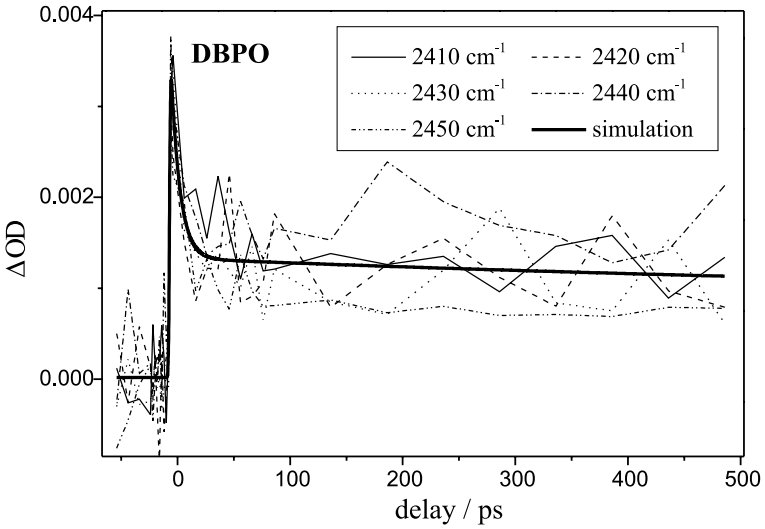

Fig. 5. Background signal to the blue of the CO_2 ν_3-band: time-dependent transient absorbance in the 2410 to 2450 cm^{-1} range after UV-induced decomposition of DBPO in CH_2Cl_2.

DBPO in CH_2Cl_2. Almost the same signals are observed in ps experiments carried out on pure CH_2Cl_2. They are assigned to transient absorption of the front window and of the solvent. The pure solvent signals cannot be used directly for correction of the transient spectra recorded during peroxide decomposition as the absorbed energy is different in both experiments. The time-dependent transients in Fig. 5 were averaged and fitted biexponentially to yield the wavelength independent transient background signal given as the intense solid line in Fig. 5. The shorter one of the two half-lives associated with the biexponential fit is 8 ± 2 ps. The second half life is in the nanosecond region. A simulated background signal is subtracted from each of the time-dependent traces recorded during the peroxide decomposition experiments.

Fig. 6 presents time-dependent traces measured for the decarboxylation of DBPO at 2335 cm^{-1} (which is the peak position at delay times $>$ 300 ps) and at 2250 cm^{-1}. The simulated background signal from Fig. 5 is included in Fig. 6. It is clearly seen, that the fast component of the background signal is significant only up to 10 ps but remains below 40% of the overall signal intensity at 2250 and 2335 cm^{-1}. After 20 ps, the background absorption gives rise to a nearly constant offset of OD = 0.001. This offset agrees well with the signal intensity at 2250 cm^{-1} and long delay times. The signal at 2335 cm^{-1} and negative delay times is primarily due to the action of atmospheric CO_2.

The time dependent signals at both 2250 and 2335 cm^{-1} reflect the spectral and temporal evolution of the CO_2 band: Toward increasing delay time, the band shifts to higher wavenumbers, resulting in an absorption decay at

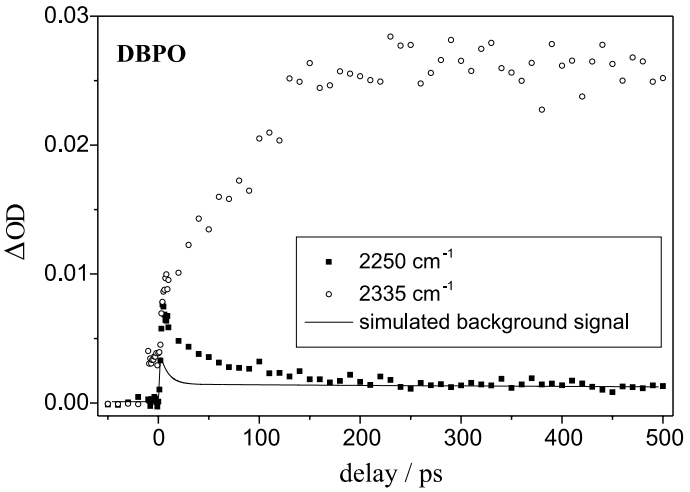

Fig. 6. Time-dependent transient absorbance at 2250 cm^{-1} and 2335 cm^{-1} after decomposition of DBPO; the solid line denotes the simulated signal from Fig. 5.

2250 cm^{-1} (after the instantaneous rise at time zero) and in an absorption increase at 2335 cm^{-1}.

Discussion

The absorption observed in the wavenumber region from 2100 to 2400 cm^{-1} (Figs. 3 and 4) is exclusively assigned to CO_2 from photolysis of the peroxides. The temporal and spectral evolution after photolysis of the asymmetric CO_2 stretching vibration (ν_3) is determined by both the mode of bond scission and, more importantly, by the energy relaxation of the vibrationally excited molecule. In order to clarify the decomposition mechanism, the integrated absorbance of the entire spectral region from 2100 to 2400 cm^{-1} will first be studied. Subsequently the band profile of the transient spectra will be investigated in an attempt to derive the internal vibrational energy of CO_2 and the time constant of vibrational relaxation in the liquid CH_2Cl_2 solvent.

A. Decomposition mechanism

In contrast to molar absorption coefficients, $\varepsilon(\tilde{\nu})$, at a fixed wavenumber $\tilde{\nu}$, which are temperature dependent, the vibrational band intensity $B = \int_{\nu_3} \varepsilon(\tilde{\nu})\mathrm{d}\tilde{\nu}$ is constant or only weakly temperature dependent [22]. Thus integrated absorbance, $B^* = \int_{\nu_3} A(\tilde{\nu})\mathrm{d}\tilde{\nu}$, may serve as a measure for CO_2 concentration. Integrated absorbances, B^*, are determined as the area under the optical density curves measured at fixed delay time.

In Fig. 7, the resulting numbers are plotted versus delay time for the photolysis of TBBC and DBPO. Subtraction of the background signal may not completely eliminate the transient background absorption within the first 10 ps of the detection period.

In Fig. 7, integrated absorbances are seen also at negative delay times. They result from effects on the pulse profile of the atmospheric CO_2 that is contained in the IR light path [20]. The transient background signal reduces the time resolution in the initial period after applying the pump pulse. The maximum value of integrated absorbance is reached within 10 ps for each of the two peroxides. A weak decay is seen toward larger delay times.

The other peroxides studied also reach maximum integrated absorbance within the first 10 ps. This type of behaviour, with respect to the available time resolution of the experimental setup, is considered as instantaneous decomposition. Absorption of CO_2 that is formed during (successive) thermal decarboxylation of intermediates on a ns – μs time scale [7] will not contribute in the time

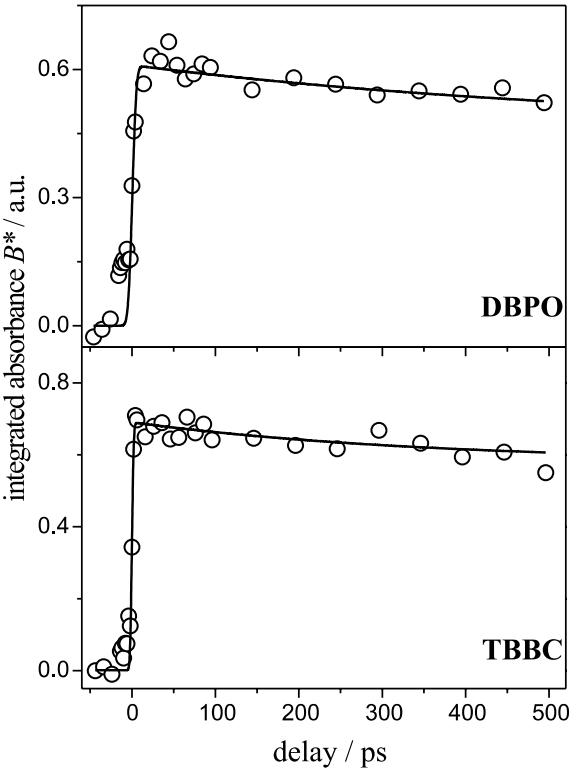

Fig. 7. Integrated absorbance of the ν_3 band of CO_2 as a function of delay time for DBPO and TBBC decomposition in CH_2Cl_2.

range up to 500 ps [4, 6]. The slight decrease of B^* in the 20 to 500 ps range (Fig. 7) most likely results from a weak temperature dependence of B.

The B^* vs. delay time data in Fig. 7 indicate that with TBBC the formation of CO_2 and thus the breaking of two bonds takes place in either a concerted or in a very fast sequential manner. With DBPO decomposition, one of the two CO_2 molecules that may be produced, is released in a similar concerted or fast sequential way whereas the second CO_2 molecule will be formed thermally on a much longer time scale. Fast CO_2 release within the first 10 ps is also seen in the UV-induced decomposition of DMBP, DNPO, TBNC and TBPB. A delayed formation of CO_2, as has been observed in the previous UV pump/IR probe study into TBNC at a pump wavelength of 308 nm, does not occur at an excitation wavelength of 248.5 nm. This difference is most likely due to the larger excess energy in the 248.5 nm experiment.

It needs to be kept in mind that the notation "concerted or very fast sequential" decomposition used within the present paper refers to the time resolution of a few picoseconds. It is obviously a matter of priority to further enhance the time resolution of the UV pump/IR probe experiment into the sub-ps range. Such efforts are currently underway.

B. Modeling of transient CO_2 spectra

The CO_2 spectra recorded at delay times up to 300 ps are due to vibrationally hot CO_2. It appears interesting to estimate the vibrational temperature from the measured ν_3-band profiles. This may be achieved via an anharmonic oscillator model presented by Hamm *et al.* [1], in which band broadening is interpreted as being due to anharmonic coupling among vibrationally excited modes. These authors pointed out that the experimental spectra may serve as a molecular thermometer for a dissolved species. Rotational excitation is not included in the model which is certainly justified under conditions where rotational relaxation is extremely fast.

The spectrum $A_k(\tilde{\omega})$ of a particular normal mode ω_k may be calculated in situations where the anharmonicity constants, x_{ik}, and the relative populations of the n levels of mode k, $a(n_k)$, are known. For the ν_3 mode of CO_2, the expression reads:

$$A_3(\tilde{\omega}) = \sum_{n_3=0}^{S} \Bigg\{ [a(n_3) - a(n_3+1)](n_3+1) \cdot \sum_{n_1=0}^{S} \sum_{n_2=0}^{S} a(n_1)\, a(n_2) \cdot g_3[\tilde{\omega} - \tilde{\nu}(n_3 \rightarrow n_3+1)] \Bigg\}, \quad (1)$$

where S is the highest vibrational level that is considered in the estimate. The calculations included vibrational levels up to $S = 10$. The line shape function, $g_3(\tilde{\nu})$, accounts for the band contour in an environment of liquid CH_2Cl_2. FTIR

studies on the ν_3 mode of CO_2 in CH_2Cl_2 at ambient temperature revealed that a Lorentzian profile with a half-width of 8 cm^{-1} is a suitable line shape function. $g_3(\tilde{\nu})$ is assumed to be independent of temperature. The populations $a(n_k)$ depend on the internal temperature of the molecule according to the Boltzmann distribution. Above 1000 K, excited levels of the (high-frequency) ν_3 mode are less populated, in contrast to the excited levels of the two low-frequency modes, ν_1 and ν_2. The contour of the overall band varies with temperature as a consequence of changes in the populations $a(n_k)$. The wavenumber $\tilde{\nu}$ for the $n_k \rightarrow n_k + 1$ transition of mode k is coupled to the other modes $i \neq k$ according to Eq. (2):

$$\tilde{\nu}(n_k \rightarrow n_k + 1) = \tilde{\omega}_k + 2x_{kk} + \sum_{i \neq k} \frac{x_{ik}}{2} + 2x_{kk} n_k + \sum_{i \neq k} x_{ik} n_i \,. \tag{2}$$

Via Eq. (1), absorbance spectra $A_3(\tilde{\omega})$ were calculated as a function of temperature. The harmonic frequencies are [23]: $\tilde{\omega}_1 = 1354.07\ cm^{-1}$, $\tilde{\omega}_2 = 672.95\ cm^{-1}$ and $\tilde{\omega}_3 = 2396.30\ cm^{-1}$; the anharmonicity constants are [24]: $x_{11} = -3.10\ cm^{-1}$, $x_{22} = 1.59\ cm^{-1}$, $x_{33} = -12.50\ cm^{-1}$, $x_{12} = -5.37\ cm^{-1}$, $x_{13} = -19.27\ cm^{-1}$ and $x_{23} = -12.51\ cm^{-1}$. A frequency shift of 11 cm^{-1} has been applied to the gas phase phase frequencies given above to adjust for the effect of solvent environment [21].

Shown in Fig. 8 is the calculated absorbance band contour (in arbitrary units) for the ν_3 band of CO_2 at 1000 K. The non-diagonal anharmonic terms strongly contribute to the overall bandshape. In addition to the maximum peak at 2336 cm^{-1} distinct side bands occur toward lower wavenumbers. As a consequence of the negative sign of the anharmonicity constants, the peak position is red-shifted relative to the spectrum taken at 300 K. The spectra calculated via Eqs. (1) and (2) were convoluted with a Lorentzian line shape function of half-width 11 cm^{-1} to account for the bandwidth of the IR probe pulse. The procedure results in a significantly broadened spectrum given by the solid line in Fig. 8.

Fig. 9 shows a series of spectra calculated for temperatures between 300 and 3300 K at intervals of 200 K. Each spectrum is convoluted with the IR pulse spectral profile. With decreasing temperature, a narrowing of the absorption band and a shift to larger wavenumbers are observed. The arrows indicate the direction of spectral change upon lowering temperature. The series of spectra resembles measured sequences of spectra as the ones shown in Fig. 3.

Comparison of simulated and measured spectra allows to assign a vibrational temperature to indiviual spectra determined at different delay times. In doing so, the temperatures for the experimental TBBC spectra in Fig. 4 taken at delay times of 20, 100, and 500 ps are obtained to be 2700 ± 200 K, 1000 ± 100 K, and 300 ± 50 K, respectively. The uncertainties in estimated (model-dependent) temperature, of about $\pm 10\%$, reflect the quality by which

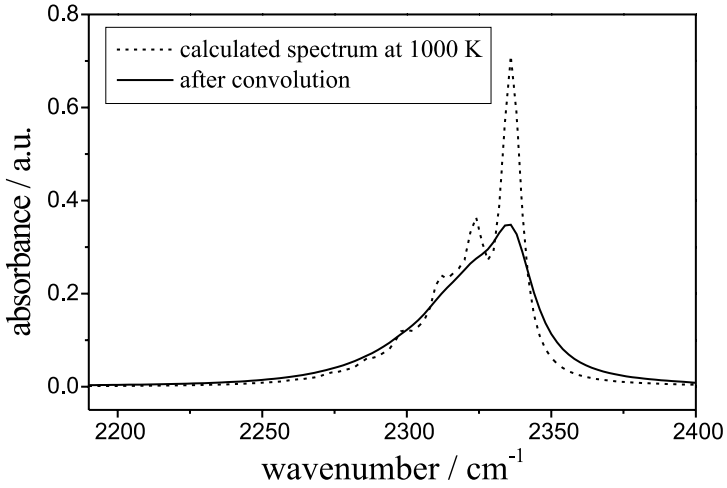

Fig. 8. Simulated CO_2 spectrum for 1000 K before and after convolution with the IR pulse profile.

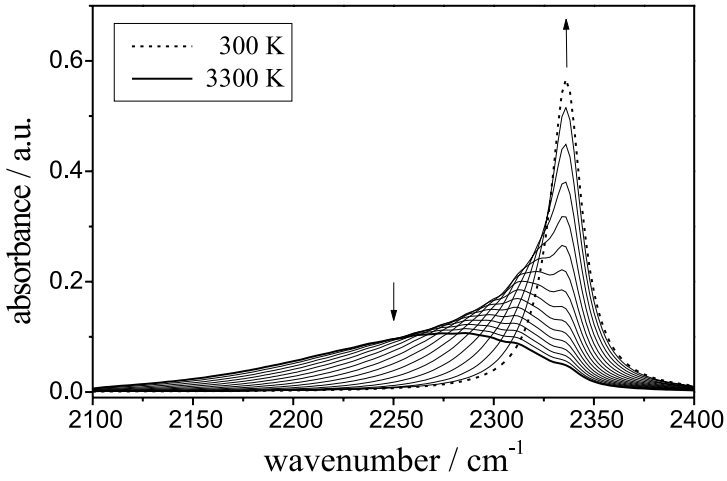

Fig. 9. Simulated CO_2 spectra (convoluted with IR pulse profile) between 300 and 3300 K, the arrows indicate the change with decreasing temperature.

the experimental spectra are simulated via the anharmonic oscillator model. The "true" temperature certainly may be off by more than ±10%. The lines in Fig. 4 are the simulated curves for 2700, 1000 and 300 K. The agreement between measured and simulated spectra is very satisfactory within the entire range of the ν_3 band. It is particularly noteworthy that the anharmonic oscillator model fully accounts for the influence of temperature on both bandshape and

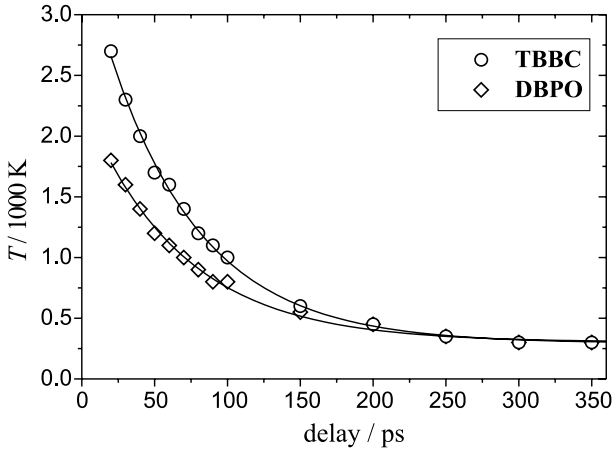

Fig. 10. Time dependence of the vibrational temperature of CO_2, released in the UV-photoinduced decomposition of TBBC and DBPO in CH_2Cl_2; the solid lines are monoexponential fits (see text).

peak position. It may be concluded that the band analysis of the CO_2 ν_3 mode indeed provides a reasonable estimate of internal temperature.

According to the procedure described above, a temperature is assigned to each of the transient spectra. The results for DBPO and TBBC are shown in Fig. 10. For both peroxides the internal temperature vs. delay time data are adequately represented by a monoexponential fit (solid lines). The relaxation half lives are 67 ± 4 ps (DBPO) and 64 ± 2 ps (TBBC). The vibrational temperatures at a delay time of 20 ps are determined to be 1800 ± 200 K (DBPO) and 2700 ± 200 K (TBBC).

In Fig. 11, the time dependence of CO_2 internal temperature after peroxide decomposition in CH_2Cl_2 is plotted for the entire set of experiments. The relaxation data clearly reflects peroxide structure. The peroxycarbonates TBBC and TBNC produce CO_2 with highest temperatures, around 2700 and 2600 K at $t = 20$ ps. For the three diacyl peroxides, the CO_2 temperature at $t = 20$ ps is in the 2000 K (DNPO and DMBP) to 1800 K (DBPO) range. For TBPB the lowest "initial" CO_2 temperature is derived, which is close to 1400 K at $t = 20$ ps. Again a monoexponential decay of temperature vs. delay time is observed. A single such decay curve (solid line in Fig. 11) is sufficient to represent the relaxation behavior of CO_2 formed in the fragmentation of peroxides which are similar in the relevant part of their molecular structure.

The monoexponential relaxation times τ and the "initial" temperatures for $t = 20$ ps as obtained from the analysis of the individual transient absorbance spectra are summarized in Table 1.

Irrespective of "initial" temperature, which varies between 1400 K (TBPB) and 2700 K (TBBC), within experimental error the cooling of vibrationally hot

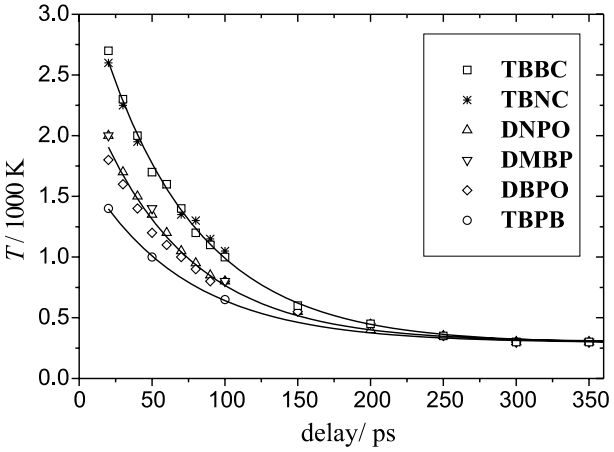

Fig. 11. Time dependence of the vibrational temperatures of CO_2, released in the UV-photoinduced decomposition in CH_2Cl_2 of the entire set of peroxides studied within the present work; the solid lines represent monoexponential fits for peroxides which belong to the same family.

CO_2 in CH_2Cl_2 occurs with a time constant of 67 ± 5 ps. This result is consistent with the observation of exclusively monoexponential cooling curves. The monoexponential cooling behavior is not surprising, since the initial temperature assigned to CO_2 corresponds to a relatively small degree of excitation of the CO_2 normal modes, i.e. more than half of the population are typically found at $n_3 = 0$, $n_2 = 1$, and $n_1 = 0$. In this range of excess energies vibrational relaxation is expected to follow a monoexponential decay [25, 26]. That such identical cooling behavior is observed, provides strong support for the internal temperature determination via the anharmonic coupling model (Eq. 1).

Consequently the "initial" temperatures at delay times of 20 ps can also be regarded with some confidence. These temperatures, which differ significantly for the three groups of peroxides, must be related to the maximum available

Table 1. Estimated temperatures T (at a delay time of 20 ps) and cooling relaxation times τ of CO_2 from peroxide decomposition.

CO_2 source	T (at $t = 20$ ps)/K	τ/ps
TBBC	2700 ± 200	64 ± 2
TBNC	2600 ± 200	70 ± 4
DNPO	2000 ± 200	64 ± 4
DMBP	2000 ± 200	67 ± 6
DBPO	1800 ± 200	67 ± 4
TBPB	1400 ± 100	69 ± 9

excess energy and the extent of vibrational energy redistribution within the peroxide molecule prior to bond scission.

Details of the photodissociation dynamics on a sub-ps scale are not accessible with the current experimental setup. Moreover, information about the electronic surface, on which the dissociation takes place, is not available. Nevertheless, a rough estimate of the maximum CO_2 temperature attainable in the reaction can be made. If one assumes that intramolecular vibrational energy redistribution (IVR) in the peroxide molecule prior to the primary dissociation step is complete, the vibrational excess energy in the ground state may be obtained from a harmonic oscillator model considering the pump photon energy [4]. With vibrational frequencies taken from ab initio calculations [27], the peroxide internal energies after excitation correspond to vibrational temperatures of the ground state, e.g., of about 1400 K for DBPO and 1300 K for TBBC. Subtraction of approximate energies associated with the dissociation of the peroxy-bond ($100\,kJ\,mol^{-1}$) and the C (α)–C (carbonyl)-bond ($30\,kJ\,mol^{-1}$) [3, 5], yields, as an upper limit for the internal temperature of CO_2 produced from fully thermalized excited peroxide molecules, values around 1100 K for both peroxides. This temperature is significantly lower than the vibrational temperatures estimated from the band profile at a delay time of 20 ps.

A reason for this discrepancy might be that dissociation occurs from a not fully thermalized state. It is, however, fairly unlikely that IVR within the peroxide molecule will take longer than a few picoseconds [11]. In addition, previous UV pump (308 nm)/IR probe experiments on TBNC showed that even in case of stepwise decomposition (where CO_2 is formed with a time constant of about 31 ps, when IVR will definitely be completed) the vibrational temperature is 1600 K above the value estimated for dissociation from a thermalized state [4].

Another explanation for the high "initial" temperature assumes that a significant fraction of the energy release, associated with linear CO_2 formation from a bent precursor species, remains in the CO_2 molecule. Rough estimates of the energy release associated with angle and bond length relaxation during CO_2 formation indicate that temperatures as high as the ones deduced from the transient spectra may easily be reached. Similar conclusions have been derived from the photodissociation at 266 nm of s-triazine where a particularly high excitation of the bending mode of the HCN product is seen [28]. Zhang and Hossenlopp investigated the photoinduced (at 222 nm) decarboxylation of perfluorinated anhydrides which leads to the formation of CO_2 [29]. Analysis of the population of the CO_2 bending levels, from 01^10 up to 04^40, yields a Boltzmann temperature of 3100 ± 1000 K whereas the vibrational temperature deduced from the asymmetric stretching mode (00^01) was noticeably lower.

The argument that the high vibrational temperatures of CO_2 essentially result from the energy associated with structural relaxation of the bent O−C−O moiety can also easily explain the very high temperatures observed after photo-decomposition (at 308 nm) of TBNC. With the O−C−O moiety and the aromatic ring being separated by two single bonds, the dissipation of excess

energy from CO_2 formation is less favored than in situations with conjugated double bonds as in the diacyl peroxides and the aromatic peroxyester. The structural relaxation argument also explains why the peroxides clearly exhibit a family-type behavior with respect to the "initial" temperature of the vibrationally hot CO_2.

Conclusion

Analysis of the transient IR spectra of CO_2 released during ps photodecomposition of several aromatic peroxides, via an excited anharmonic oscillator model, provides the time dependence of vibrational temperature. Irrespective of the type of peroxide and thus of "initial" temperature, a single monoexponential relaxation adequately describes the cooling of CO_2 in the environment of liquid CH_2Cl_2. Further peroxide decomposition experiments should be carried out with other solvents to quantify the influence of the molecular surrounding on intermolecular energy relaxation. Preliminary studies in liquid CCl_4 indicate that the relaxation rate is much slower and occurs with a time constant of about 180 ± 20 ps. Lower cooling rates in CCl_4 as compared to other chlorinated hydrocarbons have also been reported for energy relaxation of several small [12] and large [11] molecules in these solvents. The remarkably high "initial" temperatures can be best understood by assuming that the large excess energy mainly results from structural relaxation of the bent O−C−O moiety.

It appears to be a matter of priority to further improve the time resolution of the UV pump/IR probe experiment. Experiments with sub-ps time resolution are required in order to unambiguously distinguish between single bond scission and concerted two-bond scission.

Acknowledgement

This work has been generously supported by the Deutsche Forschungsgemeinschaft within the Sonderforschungsbereich 357 ("Molekulare Mechanismen unimolekularer Prozesse"). Helpful comments by Dr. D. Schwarzer are gratefully acknowledged. The authors are also grateful to AKZO NOBEL for the synthesis and provision of the peroxide samples.

References

1. P. Hamm, S. M. Ohline and W. Zinth, J. Chem. Phys. **106** (1997) 519.
2. A. Rudin, *The Elements of Polymer Science and Engineering*, Academic Press, Orlando (1982).
3. R. Hiatt, in: *Organic Peroxides*, Vol. II, ed. D. Swern, Wiley Interscience, New York (1971) 799; S. Patai, in: *The Chemistry of Peroxides*, Wiley, New York (1983);

K. Fujimori, in: *Organic Peroxides*, ed. W. Ando, Wiley, New York (1992) 319; Y. Sawaki, in: *Organic Peroxides*, ed. W. Ando, Wiley, New York (1992) 425; M. Buback and C. Hinton, Z. Phys. Chem. **193** (1996) 61; M. Buback and J. Sandmann, Z. Phys. Chem. **214** (2000) 583; and references cited in these articles.
4. J. Aschenbrücker, M. Buback, N. P. Ernsting, J. Schroeder and U. Steegmüller, Ber. Bunsenges. Phys. Chem. **102** (1998) 965.
5. U. Steegmüller, Dissertation, Göttingen (1997).
6. J. Aschenbrücker, M. Buback, N. P. Ernsting, J. Schroeder and U. Steegmüller, J. Phys. Chem. B **102** (1998) 5552.
7. S. Yamauchi, N. Hirota, S. Takahara, H. Sakuragi and K. Tokumaru, J. Am. Chem. Soc. **107** (1985) 5021; L. Grossi, J. Lusztyk and K. U. Ingold, J. Org. Chem. **50** (1985) 5882; G. C. Flowers and J. E. Leffler, J. Org. Chem. **54** (1989) 3995; D. E. Falvey and G. B. Schuster, J. Am. Chem. Soc. **108** (1986) 7419; J. Wang, T. Tateno, H. Sakuragi and K. Tokumaru, J. Photochem. Photobiol. A: Chem. **92** (1995) 53; and references cited in these articles.
8. M. Steinberg and W. O. Davies, J. Chem. Phys. **34** (1961) 1373.
9. R. H. Tourin, J. Opt. Soc. Am. **51** (1961) 175.
10. C. C. Ferriso, J. Chem. Phys. **37** (1962) 1955.
11. T. Elsaesser and W. Kaiser, Annu. Rev. Phys. Chem. **42** (1991) 83.
12. J. C. Owrutsky, D. Raftery and R. M. Hochstrasser, Annu. Rev. Phys. Chem. **45** (1994) 519.
13. A. Tokmakoff, B. Sauter, A. S. Kwok and M. D. Fayer, Chem. Phys. Lett. **221** (1994) 412; T. P. Dougherty and E. J. Heilweil, Opt. Lett. **19** (1994) 129; A. Tokmakoff and M. D. Fayer, J. Chem. Phys. **103** (1995) 2810; D. Schwarzer, J. Troe, M. Votsmeier and M. Zerezke, J. Chem. Phys. **105** (1996) 3121; P. Hamm, M. Lim and R. M. Hochstrasser, J. Chem. Phys. **107** (1997) 10523; L. K. Iwaki, J. C. Deàk, S. T. Rhea and D. D. Dlott, Chem. Phys. Lett. **303** (1999) 176; G. Seifert, R. Zürl, T. Patzlaff and H. Graener, J. Chem. Phys. **112** (2000) 6349; and references cited in these articles.
14. D. Budac and P. Wan, J. Photochem. Photobiol. A: Chem. **67** (1992) 135, and references therein.
15. J. Aschenbrücker, U. Steegmüller, N. P. Ernsting, M. Buback, J. Schroeder and J. Jasny, Appl. Phys. B **65** (1997) 441.
16. S. Szatmári and F. P. Schäfer, Opt. Commun. **68** (1988) 196.
17. T. Bultmann, D. Bingemann, N. P. Ernsting, D. Schwarzer and L. Nikowa, Rev. Sci. Instrum. **66** (1995) 4393.
18. D. S. Bethune, Appl. Opt. **20** (1981) 1897.
19. J. Jasny, Opt. Commun. **53** (1985) 238; J. Jasny, Rev. Sci. Instrum. **57** (1986) 1303.
20. M. Woerner, A. Seilmeier and W. Kaiser, Opt. Lett. **14** (1989) 636.
21. D. B. Cunliffe-Jones, Spectrochim. Acta A **25** (1969) 779.
22. M. Buback, J. Schweer and H. Tups, Z. Naturforsch. **41a** (1986) 505; M. Buback, J. Schweer and H. Tups, Z. Naturforsch. **41a** (1986) 512.
23. I. Suzuki, J. Mol. Spectrosc. **25** (1968) 479.
24. H. R. Gordon and T. K. McCubbin, J. Mol. Spectrosc. **19** (1966) 137.
25. C. Heidelbach, V. S. Vikhrenko, D. Schwarzer and J. Schroeder, J. Chem. Phys. **110** (1999) 5286.
26. I. I. Fedchenia, G. Käb and J. Schroeder, to be published.
27. Method and basis set: HF/6-31G(d) (frequencies scaled with 0.8929), Gaussian 98, Revision A.5, Gaussian, Inc., Pittsburgh PA (1998).
28. J. Park, Chem. Phys. Lett. **293** (1998) 383.
29. Y. Zhang and J. M. Hossenlopp, Chem. Phys. Lett. **275** (1997) 319.